Mechanical Systems and Signal Processing 24 (2010) 2807–2823

Contents lists available at ScienceDirect

Mechanical Systems and Signal Processing

journal homepage: www.elsevier.com/locate/jnlabr/ymssp

A simple frequency-domain algorithm for early detection of damaged gear teeth

William D. Mark [a,*], Hyungdae Lee [b], Romano Patrick [b], Joseph D. Coker [c]

[a] Applied Research Laboratory and Graduate Program in Acoustics, The Pennsylvania State University, University Park, PA 16802, USA
[b] Impact Technologies LLC, 200 Canal View Blvd, Rochester, NY 14623, USA
[c] Department of Aerospace Engineering, University of Maryland, College Park, MD 20742, USA

ARTICLE INFO

Article history:
Received 17 July 2009
Received in revised form
9 April 2010
Accepted 19 April 2010
Available online 28 April 2010

Keywords:
Gear-health monitoring
Diagnostics
Transmission error
Planetary gears
Epicyclic gears

ABSTRACT

Fixed transducers often are used to monitor meshing gear pairs in order to detect tooth damage. A simple frequency-domain damage-detection algorithm is suggested for very early detection of such damage. Ratios of rotational-harmonic amplitudes computed from before and after potential damage are utilized to eliminate effects of transducer and structural-path-caused amplitude changes between tooth-meshing location and transducer output, to minimize attenuating effects of multiple-tooth contact, and thereby, to approximately equally weight rotational-harmonic amplitudes over a wide range of harmonics. Statistical averaging of absolute values of logarithmic ratios of rotational-harmonic amplitudes is used to minimize fluctuations caused by multiple-tooth contact and manufacturing errors on the subject gear. Synchronous averaging is employed to minimize effects of noise and manufacturing errors on the mating gear. Time-windowing tailored to contact ratios of mating gears is utilized to isolate individual tooth locations. Resultant windowing effects on availability of useful rotational harmonics are analyzed. Application of the algorithm to detection of seeded bending-fatigue faults on a planetary ring-gear tooth indicates that successful detections were achieved.

1. Introduction

Consider a meshing pair of involute spur or helical gears operating at constant speed and transmitting constant torque. If the working-surface deviation from a perfect involute surface of every tooth on each of the two meshing gears is identical with no tooth-spacing errors, and the center of rotation of each of the two gears is its base cylinder axis [1, p. 489], then the static-transmission-error (STE) vibratory-excitation spectrum from such an error-free gear pair would contain only contributions to the tooth-meshing harmonics of the gear pair [2]. Suppose a tooth on one of these meshing gears develops a pit or root crack, thereby producing a geometric change in the working surface, or change in the loaded working surface of the affected tooth due to its changed elastic deformation. Such changes will cause a non-zero contribution to every STE rotational-harmonic amplitude from the affected gear [2,3], but a fractional change only of the order of $1/N$ to the tooth-meshing harmonics of the gear pair, where N is the number of teeth on the affected gear.

* Corresponding author. Tel.: +1 8148653922; fax: +1 8148636185.
E-mail addresses: wdm6@only.arl.psu.edu, wdm6@psu.edu (W.D. Mark), Hyungdae.Lee@impact-tek.com (H. Lee), Romano.Patrick@impact-tek.com (R. Patrick), jcoker@umd.edu (J.D. Coker).

0888-3270/$ - see front matter © 2010 Elsevier Ltd. All rights reserved.
doi:10.1016/j.ymssp.2010.04.004

However, the teeth of all real gears have (small) tooth-to-tooth variations in their working surfaces caused by manufacturing errors, including tooth-spacing errors. The manufacturing error on each tooth also will produce a contribution to every STE rotational-harmonic amplitude from that gear [2]. The superposition of these rotational-harmonic STE contributions caused by manufacturing errors on the N teeth normally would mask the rotational-harmonic contributions caused by early damage on a single tooth or on a small number of teeth. Hence, the suggested damage-detection algorithm utilizes statistical averages over many rotational harmonics to detect fractional changes in individual rotational-harmonic amplitudes caused by damage.

Because the manufacturing error on each tooth produces a (complex) contribution to all rotational-harmonic amplitudes, and there are N such complex contributions to each rotational harmonic, the (complex) contribution to each rotational harmonic caused by early damage on a single tooth, or on a small number of teeth, will cause either an increase or decrease [2,3] in each real rotational-harmonic amplitude with almost equal probability, unless the subject gear teeth contain virtually no manufacturing errors. Hence, the suggested damage-detection algorithm is formulated to detect with equal weight, either increases or decreases of individual rotational-harmonic amplitudes caused by potential tooth damage.

The fundamental basis for the work reported on herein is the static-transmission-error vibratory excitation of meshing gear pairs [2–9]. Also fundamental is the contribution to individual-gear STE rotational-harmonic amplitudes caused by manufacturing errors [2]. These STE rotational-harmonic contributions are sometimes referred to as the residual signal [10,11]. Synchronous averaging [12–15] utilizing the number of contiguous gear rotation segments equal to an integer multiple of the number of teeth on the mating gear [16] is also critical for maximum elimination of rotational-harmonic contributions from the gear that mates with the gear of interest. Windowing [17,18] is used to isolate the STE contributions of individual teeth thereby enhancing detectability.

Such isolation also can be accomplished by using time–frequency analysis of the Wigner–Ville distribution and wavelets [18–25]. Some studies have focused on the amplitude and frequency or phase modulation effects [3,26–29] arising from changes in mesh stiffness [30,31] caused by tooth-root cracks or plastic deformation [16]. The fact that gears are circular causing periodic behavior of their vibratory excitations has led to cyclostationary modeling [32] of these vibrations [33,34].

2. Vibratory excitation and transducer response

2.1. STE vibratory excitation

The STE vibration excitation of a meshing parallel-axis gear pair, including the excitation contributions from manufacturing errors, is derived in [2,7], summarized in [9], and summarized with emphasis on application to gear-health monitoring in [16]. There are three principal sets of harmonics in this STE vibration excitation: the tooth-meshing harmonics of the gear pair and rotational-harmonic sets from each of the two meshing gears. If N is the number of teeth on a gear and P is its rotation period, then the tooth-meshing fundamental period is P/N. Because of the way in which gears mesh with one another, the tooth-meshing harmonics and their fundamental periods are common to both gears of a meshing pair. Denote, by superscripts, gears (1) and (2) of a meshing pair. Since their tooth-meshing fundamental periods coincide, it follows that:

$$\frac{P^{(1)}}{N^{(1)}} = \frac{P^{(2)}}{N^{(2)}} \tag{1a}$$

or

$$N^{(1)}P^{(2)} = N^{(2)}P^{(1)}. \tag{1b}$$

The fundamental periods of the rotational harmonics of the two gears (1) and (2) are their rotation periods $P^{(1)}$ and $P^{(2)}$, which are $N^{(1)}$ and $N^{(2)}$ times their tooth-meshing fundamental periods $P^{(1)}/N^{(1)}$ and $P^{(2)}/N^{(2)}$, respectively. Therefore, the tooth-meshing fundamental harmonics of gears (1) and (2) are the $N^{(1)}$th and $N^{(2)}$th rotational harmonics, respectively, of the two gears.

The subject of this paper is detection of very early damage on one or a small number of teeth on a gear. The STE tooth-meshing harmonics are generated from the mean deviations of the loaded tooth working surfaces of the two meshing gears. Therefore, very early damage on one or a small number of teeth on a gear will cause only a small change in the tooth-meshing-harmonic amplitudes of the STE vibratory excitation.

The remaining rotational-harmonic contributions of each gear to the STE vibratory excitation are caused by the collective deviations of the individual loaded tooth working surfaces on that gear from the loaded mean deviation of the working surfaces of that gear. Because the manufacturing goal is normally to produce gears with identical tooth working surfaces, any damage to a working surface, or change in stiffness of a tooth will, in principle, affect the STE rotational-harmonic amplitudes from that gear more than the tooth-meshing harmonic amplitudes. Moreover, for each tooth-meshing harmonic amplitude available for damage-detection purposes, there are $N-1$ rotational-harmonic amplitudes available, which can be utilized for statistical averaging. Furthermore, the STE tooth-meshing harmonic amplitudes are strongly dependent on gear loading, but the remaining STE rotational-harmonic amplitudes are only weakly dependent on

gear loading. Hence, changes in the STE tooth-meshing harmonic amplitudes caused by unintentional loading variations might be mistaken as having been caused by gear damage, while such "false-alarms" are less likely to be caused by utilizing the STE rotational-harmonic amplitudes for damage detection. Therefore, the rotational-harmonic amplitudes will be utilized in the detection algorithm described in the following pages.

2.2. Transducer response

Gear-health monitoring normally is implemented by a fixed transducer that responds to the vibration signal generated by a meshing gear pair of interest. A structural transmission path exists between the tooth-meshing vibration-excitation location and transducer location. Consequently, even if the vibration signal caused by tooth damage were known, the transducer output signal caused by the damage signal would be significantly changed by both the structural-path and the transducer-response signal distortions. However, normally, this combined structural-path and transducer-response function is accurately characterized as a linear time-invariant system, but with unknown impulse-response and frequency-response properties. Therefore, the frequency locations of the rotational-harmonic contributions caused by a damaged-tooth vibration signal will remain unaffected by this combined structural/transducer-response function, as will its *approximate* time location, but with significant temporal distortion and dispersion.

If carried out correctly [16], synchronous averaging of the transducer response will virtually eliminate the interference effects of both additive noise and the manufacturing error contributions from one of the two meshing gears, thereby leaving only the STE vibration-excitation contributions from the tooth-meshing harmonics of the gear pair and the rotational harmonics from the other of the two meshing gears. Denote by $N^{(1)}$ the number of teeth on the gear to be investigated for tooth damage, and by $N^{(2)}$ the number of teeth on the mating gear. For the case of hunting-tooth gear pairs ($N^{(1)}$ and $N^{(2)}$ possess no common integer divisor except unity), if the synchronous average of the transducer-response waveform consists of the average of $N^{(2)}$ contiguous segments or an integer multiple of $N^{(2)}$ contiguous segments, where each segment is of duration equal to the rotation period of gear (1), then the Fourier series spectrum of this synchronous average will contain [2,16] only the tooth-meshing harmonics of the gear pair and the rotational-harmonic contributions from gear (1), which is the gear of interest. For non-hunting-tooth gear pairs, this spectrum will contain some rotational-harmonic contributions from gear (2).

3. Frequency analysis of transducer response

3.1. Manufacturing-error contributions

Manufacturing errors on the tooth working surfaces of a gear can be approximately categorized into three classes: (1) the manufacturing-error component common to all teeth on the gear, (2) manufacturing errors with strong correlations over multiple-tooth spans, and (3) manufacturing errors with weak or negligible correlations over multiple-tooth spans. Manufacturing errors (and intentional tooth modifications) in class (1) provide STE contributions only to the tooth-meshing harmonics; manufacturing errors in class (2) provide STE contributions primarily to the very-low-order rotational harmonics and "sideband" rotational harmonics in the immediate neighborhoods of the tooth-meshing harmonics; whereas, manufacturing errors in class (3) generally provide weak contributions distributed to the rotational harmonics that are observed in the rotational-harmonic spans between the groups of "sideband" harmonics associated with the tooth-meshing harmonics. The typical amplitudes of the geometric manufacturing errors in the class (3) do not differ significantly from the amplitudes of early tooth damage, or changes in tooth elastic deformations caused by tooth or gear-body fatigue cracks. The tooth-working-surface manufacturing errors in class (3) constitute the "interference" that a successful damage-detection algorithm must discriminate against.

As originally shown in [2, Eqs. (131)–(135)], each such class (3) manufacturing error on every tooth provides a contribution to all STE vibratory-excitation rotational harmonics from that gear. The resultant rotational-harmonic amplitude contribution from the error on each tooth is dependent on the tooth-error amplitude; the rotational-harmonic phase from that error is dependent on the tooth-number location of that tooth and the error-attenuating effects caused by multiple-tooth contact of the meshing teeth. Therefore, for each rotational harmonic of the STE vibratory excitation, its complex amplitude is the superposition of the complex-amplitude contributions from all of the tooth errors, and its phase is the resultant phase determined by the superposition of these complex amplitudes. The class (3) manufacturing error on each tooth provides a contribution to every STE rotational harmonic. See Appendix A and, e.g., [3, Eq. (A.4)].

3.2. Tooth-damage contributions

Exactly in the same way that the weakly correlated class (3) manufacturing errors contribute to the STE rotational harmonics, the initial damage, or change in tooth-stiffness, of a single tooth provides a contribution to every STE vibratory-excitation rotational harmonic. But the class (3) manufacturing errors on all of the N teeth also provide contributions to every STE rotational harmonic. Therefore, the fractional change in each rotational harmonic caused by damage on one or a few teeth will be small, and because of the above-described phase behavior, the change in amplitude of any particular

rotational harmonic caused by initial damage on one or a small number of teeth can result in either an increase of decrease in that harmonic amplitude, as described in Appendix A. This behavior suggests that a frequency-domain early-detection algorithm of damaged teeth should look for changes, either increases or decreases, in the individual amplitudes of the transducer-response rotational harmonics. The fractional changes will be the largest in the above-described rotational-harmonic spans between the groups of "sideband" harmonics associated with the tooth-meshing harmonics. This is the STE vibratory-excitation rotational-harmonic region where only the class (3) manufacturing errors (and tooth-damage) provide contributions. Because the fractional changes in these rotational-harmonic amplitudes caused by early damage are expected to be small, all available rotational-harmonic regions dominated by only the class (3) manufacturing errors should be utilized. Several such rotational-harmonic spans are available; each such span lies between two adjacent tooth-meshing harmonics (and associated "sidebands").

3.3. Deconvolution of structural path/transducer

There is an additional benefit to dealing with fractional changes in the amplitudes of the individual rotational harmonics. Let $\alpha_\zeta(n)$ and $\alpha_y(n)$ denote, respectively, the complex Fourier series coefficients of the nth rotational harmonic of the STE vibratory excitation $\zeta(x)$ and transducer response $y(x)$, and $H(n)$ the complex-frequency-response function of the combined structural path and transducer, evaluated at rotational-harmonic frequency, n. Then,

$$\alpha_y(n) = H(n)\alpha_\zeta(n). \tag{2}$$

Complex Fourier series coefficients of synchronous averages satisfy this same relationship. Denote by subscripts b and a, synchronous average results, as described above, obtained before "b" and then after "a" attempted detections of tooth damage. Assume negligible changes in the structural path and transducer take place during this time interval. Then, from Eq. (2),

$$\frac{\alpha_y(n)_a}{\alpha_y(n)_b} = \frac{\alpha_\zeta(n)_a}{\alpha_\zeta(n)_b} \tag{3}$$

and for real amplitudes,

$$\frac{|\alpha_y(n)|_a}{|\alpha_y(n)|_b} = \frac{|\alpha_\zeta(n)|_a}{|\alpha_\zeta(n)|_b}. \tag{4}$$

That is, by dealing with *fractional changes* in the *individual* rotational-harmonic amplitudes, the effects of the structural path and transducer are removed.

The simultaneous multiple-tooth-contact of helical gears and of high-contact-ratio spur gears, e.g., internal gears, have a very substantial attenuating effect on tooth errors (and tooth damage), such that the STE contributions from these tooth deviations typically are much smaller than the actual tooth deviations. Although different error forms are attenuated somewhat differently [7,9], by dealing with the ratios of Eqs. (3) and (4), *some* of these attenuating effects on the tooth deviations are eliminated in the same manner that the effects of the structural path/transducer effects $H(n)$ are eliminated.

3.4. Basic detection metric

A metric that exactly equally weights either increases or decreases in the transducer-response individual rotational-harmonic amplitudes $|\alpha_y(n)|$ is the absolute value of the logarithm of the ratio of harmonic amplitudes, Eq. (4),

$$\left|\log\frac{|\alpha_y(n)|_a}{|\alpha_y(n)|_b}\right| = |\log|\alpha_y(n)|_a - \log|\alpha_y(n)|_b|. \tag{5}$$

The ratio of harmonic amplitudes can be expressed as

$$\frac{|\alpha_y(n)|_a}{|\alpha_y(n)|_b} = \frac{|\alpha_y(n)|_b + |\alpha_y(n)|_a - |\alpha_y(n)|_b}{|\alpha_y(n)|_b} = 1 + \frac{\delta|\alpha_y(n)|}{|\alpha_y(n)|_b}, \tag{6}$$

where

$$\delta|\alpha_y(n)| = |\alpha_y(n)|_a - |\alpha_y(n)|_b. \tag{7}$$

In the very early stages of tooth damage, only a small fractional change $\delta|\alpha_y(n)|/|\alpha_y(n)|_b$ typically will occur. But the natural logarithm to the base e=2.71828… of $(1+x)$ has the expansion

$$\log_e(1+x) = x - \frac{x^2}{2} + \frac{x^3}{3} - \frac{x^4}{4} + \cdots, \tag{8}$$

which is zero for x=0, and is monotonically increasing in x. Comparison of Eqs. (5)–(8) suggests use of the natural logarithm in the metric, Eq. (5). Quantities $\delta|\alpha_y(n)|$ and x in Eqs. (6)–(8) can be either positive or negative; however, the outer absolute-value indicator in Eq. (5), when applied to Eq. (8), ensures that the magnitude $|\delta|\alpha_y(n)||/|\alpha_y(n)|_b$ of the incremental fractional change $\delta|\alpha_y(n)|/|\alpha_y(n)|_b$ always can be regarded as non-negative.

Table 1
Illustrating outlier avoidance of ALR detection metric, Eq. (9).

$\frac{\lvert\alpha_y(n)\rvert_a}{\lvert\alpha_y(n)\rvert_b}$	1.01	1.05	1.1	1.5	2	3	6	12
$\log_e \frac{\lvert\alpha_y(n)\rvert_a}{\lvert\alpha_y(n)\rvert_b}$	0.00995	0.0488	0.0953	0.405	0.693	1.0986	1.792	2.485

As mentioned above, to achieve statistical reliability, all available transducer-response rotational-harmonic amplitudes caused by class (3) manufacturing errors from the gear under consideration should be utilized in attempted damage detections. Hence, for small fractional changes $|\delta|\alpha_y(n)||/|\alpha_y(n)|_b$, forming the average over class (3) rotational harmonics n of the natural logarithm version of the metric, Eq. (5), i.e.,

$$ALR \triangleq \underset{over\ n}{average} \left|\log_e \frac{|\alpha_y(n)|_a}{|\alpha_y(n)|_b}\right|, \tag{9}$$

will yield, approximately, the average of these fractional changes $|\delta|\alpha_y(n)||/|\alpha_y(n)|_b$,

$$ALR \approx \underset{over\ n}{average} \left|\frac{\delta|\alpha_y(n)|}{|\alpha_y(n)|_b}\right|, \quad \frac{|\delta|\alpha_y(n)||}{|\alpha_y(n)|_b} \ll 1. \tag{10}$$

Therefore, values of the quantity ALR, Eq. (9), significantly larger than zero are an indication of damage on one or more teeth on the gear under consideration, as explained below.

As described above, each synchronous-averaged transducer-response complex rotational harmonic $\alpha_y(n)$ caused by class (3) manufacturing errors is the result of a superposition of complex amplitudes caused by manufacturing errors on all teeth on the gear, e.g., Appendix A and [3, Eq. (A.4)]. Because of the virtually random phases associated with these manufacturing-error contributions, the contributions $|\alpha_y(n)|_b$ for one or a few rotational harmonics may be abnormally small, yielding a ratio $|\delta|\alpha_y(n)||/|\alpha_y(n)|_b$ not small in comparison with unity. The effect of using the (natural) logarithm in the ratios in Eqs. (5) and (9) is to substantially underweight these "outlier" harmonic contributions so that they will not dominate the average value, ALR, Eq. (9). This underweighting is illustrated in Table 1. For small differences between $|\alpha_y(n)|_a$ and $|\alpha_y(n)|_b$, the first (linear) term in Eq. (8) provides a good approximation, but for changes in $|\alpha_y(n)|$ larger than about 50 percent, the logarithm of the amplitude ratios substantially underweights the differences, thereby preventing one or a few outlier harmonics from dominating the average, Eq. (9). An alternative [35] to utilizing the average formed in Eq. (9) would be to utilize instead, the median of the quantities given by the natural logarithm version of Eq. (5), MLR, which would minimize the possibility of outlier harmonic ratios dominating the computed median detection metric.

How might the detection metric, Eq. (9), or its median counterpart, MLR, be used in an application? After a subject meshing gear pair is "run in" to eliminate the effects of removal of manufacturing asperities, etc., but before the likelihood of any significant damage, one or both of these detection metrics would be computed a substantial number of times to establish a statistical distribution of each metric for a healthy gear pair, thereby allowing a damage-detection threshold to be set that would minimize "false-alarms." Later, during system operation, one or more exceedances of this threshold would be an indication that damage had taken place. Sequentially increasing exeedances beyond the threshold would be a strong indication of damage.

4. Windowing for enhanced damage detectability

Assume an integer multiple of $N^{(2)}$ contiguous gear (1) rotation segments of the transducer response have been "stacked" and averaged to obtain an optimal synchronous average of the transducer-response contribution arising from the STE vibration excitation of gear (1), as described above and in [16]. If a sufficient number of segments are utilized in the synchronous average, then the principal remaining "interference" contribution will be the above-described manufacturing errors on gear (1), the gear of interest. "Time" windowing can be utilized, in either time or frequency-domain analysis, to minimize the interference effects of such manufacturing errors, except the effects of those errors within the immediate windowed tooth region under examination. Hence, a sequence of such window-function examinations can be used to implement examination of all teeth on the gear. This procedure is especially useful for obtaining early damage detections on gears with a large number of teeth.

4.1. Tooth-region localization

A temporal variable is required that describes the rotational position of the gear of interest. Let x denote the "roll distance" of the gear, measured on the base circle [1]. If Δ denotes the base pitch (tooth spacing on the base circle), then the circumference of the gear, measured in units of x, is $N\Delta$, where N is the number of teeth. Hence, the fundamental rotation period of the gear, in the variable x, is $N\Delta$.

Let $\sigma(x-x_k)$ denote a window function centered at roll-distance location $x=x_k$. Requirements for a suitable window function are that it be a generally non-negative function of finite duration with no discontinuities and no discontinuities in its first derivative, thereby yielding good frequency resolution, which will be seen to be a required property. With

$$\xi = x - x_k, \tag{11}$$

a function meeting these requirements is

$$\sigma(\xi) \triangleq \begin{cases} \frac{1}{2}\left[1+\cos\left(\frac{2\pi\xi}{S}\right)\right], & (-S/2) < \xi < (S/2), \\ 0, & \text{otherwise}, \end{cases} \tag{12}$$

which is of total non-zero "duration" S. Another requirement of $\sigma(\xi)$ is that it be periodic with the gear rotation period $N\Delta$, where $S < N\Delta$. The window function, Eq. (12), is called a Hann or Hanning window function. As defined by Eq. (12), the window function is centered at $\xi=0$, but when utilized, it will be centered sequentially at roll-distance values x_k, as indicated by Eq. (11).

The Fourier series coefficients of $\sigma(\xi)$, Eq. (12), are shown in Appendix B to be

$$\gamma_\sigma(n) = \frac{1}{N\Delta}\int_{-N\Delta/2}^{N\Delta/2} \sigma(\xi)\exp[-i2\pi n\xi/(N\Delta)]\, d\xi, \quad n = 0, \pm 1, \pm 2, \cdots \tag{13a}$$

$$\gamma_\sigma(n) = \frac{\sin[\pi(S/\Delta)(n/N)]}{2\pi n\{1-[(S/\Delta)(n/N)]^2\}}, \quad n = 0, \pm 1, \pm 2, \cdots \tag{13b}$$

which asymptotically decays as $1/n^3$, thereby providing good frequency resolution. By defining the normalized frequency variable,

$$\Omega \triangleq (S/\Delta)(n/N), \tag{14}$$

the Fourier series coefficients, Eq. (13), can be expressed as a function of the single variable Ω, i.e.,

$$\frac{\gamma_\sigma(n)}{S/(2N\Delta)} = \frac{\sin(\pi\Omega)}{\pi\Omega(1-\Omega^2)}. \tag{15}$$

The right-hand side of Eq. (15) is displayed in Fig. 1.

When the subject gear meshes with a mating gear, any single tooth pair will be in continuous contact over a "short" roll-distance span. In order for the window function $\sigma(\xi)$ to facilitate detection of a change in any given tooth on the subject gear, it needs to be of significant amplitude over the roll-distance span where a tooth on the subject gear is in contact, but small or zero over the remaining roll-distance span where this tooth is not in contact, thereby eliminating the interference effects caused by manufacturing errors on those teeth of the subject gear not in contact during the roll-distance span. The roll-distance contact span for any one tooth is $(Q_t+Q_a)\Delta$, where Q_t and Q_a are, respectively, the transverse (profile) and axial (face) contact ratios of the meshing gear pair [1,3]. For spur gears, $Q_a=0$. (Q_t+Q_a is sometimes called the "total contact ratio.") The window function $\sigma(\xi)$ is between 3/4 and 1 for a span in ξ of $S/3$. Therefore, to resolve potential damage on a single tooth, S should be chosen to satisfy $(S/3) \approx (Q_t+Q_a)\Delta$, or possibly somewhat larger to accommodate the time dispersion caused by the structural transmission path and transducer. With this choice of S, the window function $\sigma(\xi)$ will be between 3/4 and 1 over the roll-distance interval where a single damaged tooth is affecting the transducer response, thereby resolving the roll-distance interval affected by the damaged tooth, yet reducing or eliminating the contributions of manufacturing errors from the remaining teeth on the gear. However, for spur gears with $Q_t < 2$ and a small number of teeth, it is shown in the following pages that S should be taken somewhat larger than $3Q_t\Delta$.

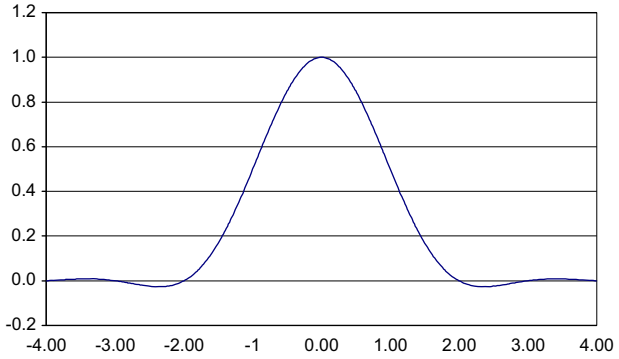

Fig. 1. Fourier representation of $\gamma_\sigma(n)$ given by right-hand side of Eq. (15) as a function of normalized frequency Ω, Eq. (14).

To examine the potential for damage on all teeth of the subject gear, the window-function will need to be shifted in roll distance x by steps of about $S/4$. If this procedure is carried out, and $S=3(Q_t+Q_a)\Delta$, as described above, then the required number of window positions to examine for damage on all teeth of the gear would be about

$$N\Delta/(S/4)=(4/3)N/(Q_t+Q_a).$$

For any widow-function position x_k, let the product of the window function $\sigma(x-x_k)$ and the synchronous-averaged transducer response $y(x)$ be denoted by

$$z(x;x_k)\triangleq\sigma(x-x_k)y(x), \tag{16}$$

and the complex Fourier series coefficient of $z(x;\,x_k)$ by $\alpha_z(n;\,x_k)$,

$$\alpha_z(n;x_k)\triangleq\frac{1}{N\Delta}\int_{-N\Delta/2}^{N\Delta/2}z(x;x_k)\exp[-i2\pi nx/(N\Delta)]\,dx, \tag{17a}$$

$$\alpha_z(n;x_k)=\frac{1}{N\Delta}\int_{-N\Delta/2}^{N\Delta/2}\sigma(x-x_k)y(x)\exp[-i2\pi nx/(N\Delta)]\,dx. \tag{17b}$$

As described above, to examine the subject gear for damage on all of its teeth, an approximate number $((4/3)N)/(Q_t+Q_a)$ of products $z(x;\,x_k)$ would be required, which would be evaluated successively at an approximate number $((4/3)N)/(Q_t+Q_a)$ of locations x_k, equally spaced in intervals of x of about $S/4$ roll-distance units apart. For each of these locations x_k, the detection metric ALR, Eq. (9), would be evaluated as before, with absolute values $|\alpha_z(n;\,x_k)|_b$ and $|\alpha_z(n;\,x_k)|_a$ replacing, respectively, $|\alpha_y(n)|_b$ and $|\alpha_y(n)|_a$. Values of ALR consistently larger at a particular x_k, say x'_k, relative to values of ALR at other x_k, would indicate damage on teeth at the roll distance location x'_k. A threshold could be established to implement such detections.

4.2. Tooth-region localization using frequency analysis

It is shown below that, for each roll-distance location x_k of the window function $\sigma(x-x_k)$, the complex Fourier series coefficients $\alpha_z(n;\,x_k)$ of the localized synchronous-averaged response $z(x;\,x_k)=\sigma(x-x_k)y(x)$, Eq. (16), can be computed entirely in the frequency domain.

The Fourier series coefficients $\alpha_y(n')$ of the previously described synchronous-averaged transducer response $y(x)$ are

$$\alpha_y(n')=\frac{1}{N\Delta}\int_{-N\Delta/2}^{N\Delta/2}y(x)\exp[-i2\pi n'x/(N\Delta)]\,dx; \tag{18}$$

hence,

$$y(x)=\sum_{n'=-\infty}^{\infty}\alpha_y(n')\exp[i2\pi n'x/(N\Delta)], \tag{19}$$

where N is the number of teeth on the gear under consideration. Substituting Eq. (19) into Eq. (17b) gives

$$\begin{aligned}\alpha_z(n;x_k)&=\frac{1}{N\Delta}\int_{-N\Delta/2}^{N\Delta/2}\sigma(x-x_k)\sum_{n'=-\infty}^{\infty}\alpha_y(n')\exp[i2\pi n'x/(N\Delta)]\exp[-i2\pi nx/(N\Delta)]\,dx\\&=\sum_{n'=-\infty}^{\infty}\alpha_y(n')\frac{1}{N\Delta}\int_{-N\Delta/2}^{N\Delta/2}\sigma(x-x_k)\exp[-i2\pi(n-n')x/(N\Delta)]\,dx\\&=\sum_{n'=-\infty}^{\infty}\alpha_y(n')\gamma_\sigma(n-n';x_k),\end{aligned} \tag{20}$$

where with $m=n-n'$, $\gamma_\sigma(m;\,x_k)$ has been defined as

$$\gamma_\sigma(m;x_k)\triangleq\frac{1}{N\Delta}\int_{-N\Delta/2}^{N\Delta/2}\sigma(x-x_k)\exp[-i2\pi mx/(N\Delta)]\,dx. \tag{21}$$

Let $\xi=x-x_k$, as in Eq. (11). Then $x=\xi+x_k$ and $dx=d\xi$, since x_k is a constant. Because, by definition, $\sigma(\xi)$ is periodic with period $N\Delta$, as in Eq. (12), there follows from Eq. (21),

$$\begin{aligned}\gamma_\sigma(m;x_k)&=\frac{1}{N\Delta}\int_{-N\Delta/2}^{N\Delta/2}\sigma(\xi)\exp[-i2\pi m(\xi+x_k)/(N\Delta)]\,d\xi\\&=exp[-i2\pi mx_k/(N\Delta)]\gamma_\sigma(m),\end{aligned} \tag{22}$$

where $\gamma_\sigma(m)$, with $m=n$, is defined by Eq. (13a), and no change in the limits of integration was required because $\sigma(\xi)$ is periodic with period $N\Delta$.

An alternative representation of $\alpha_z(n;\,x_k)$ can be obtained by using $m=n-n'$ in Eq. (20); hence, $n'=n-m$. For any given n, the infinite summation over n' in Eq. (20) becomes an infinite summation over m. Hence, instead of Eq. (20), one has with

the above-described change of variable

$$\alpha_z(n;x_k)=\sum_{m=-\infty}^{\infty}\alpha_y(n-m)\gamma_\sigma(m;x_k)$$
$$=\sum_{m=-\infty}^{\infty}\alpha_y(n-m)\exp[-i2\pi m x_k/(N\Delta)]\gamma_\sigma(m), \tag{23}$$

according to Eq. (22), where $\gamma_\sigma(m)$ is given by Eq. (13) with $n=m$.

Once the complex Fourier series coefficients $\alpha_y(n')$ of the rotational-harmonic contributions from the gear of interest of a meshing pair are computed from the synchronous-averaged transducer response, $y(x)$, as described above, the complex Fourier series coefficients of the rotational-harmonic contributions arising from each locally resolved tooth region, centered at $x=x_k$, of the transducer response can be computed by Eq. (23) using the Fourier series representation $\gamma_\sigma(n)$, for $n=m$, of the window function given by Eq. (13). The strong asymptotic decay of $\gamma_\sigma(m)$ given by Eq. (13b) with $n=m$, which decays as $1/m^3$, guarantees that $\alpha_z(n;x_k)$ will contain significant contributions from the harmonics of $\alpha_y(n-m)$ in only a limited harmonic-number region in the neighborhood of harmonic number n, as illustrated next.

4.3. Rotational-harmonic regions useful for damage detection

As described above, the rotational-harmonic regions useful for detecting a damaged tooth are only those regions that exhibit the weak rotational-harmonic amplitudes normally caused by class (3) working-surface manufacturing errors. These regions exclude the tooth-meshing harmonic locations and the so-called "sideband" locations normally found in the immediate neighborhoods of the tooth-meshing harmonics. These useful rotational-harmonic regions are delineated below, with the aid of Fig. 2, which illustrates the rotational-harmonic span of a gear's transmission-error spectrum between two adjacent tooth-meshing harmonic locations $n=pN$ and $n=(p+1)N$, where n and p denote, respectively, rotational-harmonic number and tooth-meshing harmonic number, and N is the number of teeth on the subject gear.

From Fig. 1 it is seen that the nominal half-width of $\gamma_\sigma(n)$ of Eqs. (13)–(15) is

$$\Omega=\frac{S}{\Delta}\frac{n}{N}=2; \tag{24}$$

hence, the nominal half-width of $\gamma_\sigma(n)$, in rotational harmonic n, is

$$n=2N\Delta/S. \tag{25}$$

It therefore follows from Eqs. (20)-(23) that, for any roll-distance location x_k of the window function $\sigma(x-x_k)$ centered at $x=x_k$, the Fourier series rotational-harmonic contributions of the windowed transducer response $z(x;x_k)$, Eq. (16), will have negligible contributions from the tooth-meshing harmonics $n=pN$ and $n=(p+1)N$, and closest sidebands, within the approximate harmonic-number region FN sketched in Fig. 2. Hence, F denotes the *approximate* fraction of the available $N-1$ rotational harmonics between adjacent tooth-meshing harmonics, $n=pN$ and $n=(p+1)N$, that are negligibly affected by the tooth-meshing harmonics and closest sideband harmonics at the two ends of the region. It follows directly from Fig. 2 that

$$\frac{N}{2}-\frac{FN}{2}=\frac{2N\Delta}{S}, \tag{26}$$

which can be solved for F to yield

$$F=1-\frac{4\Delta}{S}. \tag{27}$$

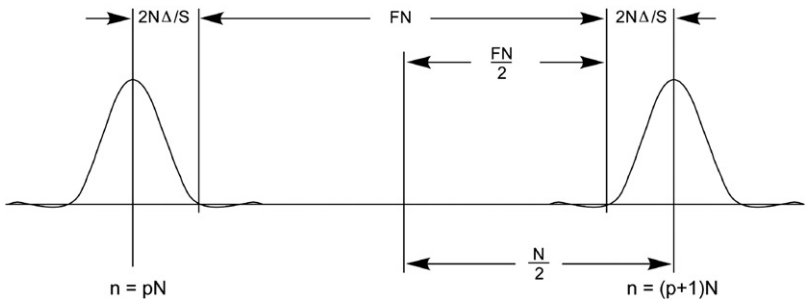

Fig. 2. Rotational-harmonic span of transmission-error spectrum between two adjacent tooth-meshing harmonic locations $n=pN$ and $n=(p+1)N$, where n and p denote, respectively, rotational-harmonic number and tooth-meshing harmonic number, and N is number of teeth. FN is rotational-harmonic number span useful for detection of tooth damage, and F is approximate fraction of the $N-1$ rotational harmonics between $n=pN$ and $n=(p+1)N$ useful for detections.

However, it was shown above that for the window-function $\sigma(\xi)$ to resolve most of the change in transmission error caused by a single damaged tooth, one should take

$$S \approx 3(Q_t + Q_a)\Delta. \tag{28}$$

Combining Eqs. (27) and (28) yields the approximate fraction F of rotational harmonics available for damage-detection purposes between any two adjacent tooth-meshing harmonics,

$$F = 1 - \frac{4}{3(Q_t + Q_a)}. \tag{29}$$

Table 2 lists F as a function of "total contact ratio" Q_t+Q_a, and as a function of S/Δ, Eqs. (27)–(29), for a range of values of Q_t+Q_a.

It follows from Table 2 that the span S of the window function $\sigma(\xi)$, Eq. (12), always must be taken larger than 4Δ to achieve a positive value of F. This normally is a limitation only for spur gears, which have zero axial contact ratios Q_a. For any values of p=0, 1, 2,…, between any two adjacent tooth-meshing-harmonic locations, $n=pN$ and $n=(p+1)N$, there are $N-1$ rotational-harmonic locations, where N is the number of teeth on the gear under consideration. Therefore, for any fractional value F, as described above, there are more rotational harmonics available for detection of damaged teeth for a gear with a large number N of teeth than for a gear with a small number of teeth. However, several to many such spans p=0, 1, 2,… are available for damage detections, and all such spans should be utilized. For each roll-distance location x_k, all available rotational harmonics from all spans within the approximate span FN in Fig. 2 should be utilized in evaluating the detection metric ALR, Eq. (9), from the absolute values $|\alpha_z(n; x_k)|$, as described earlier.

As mentioned above, for spur gears with transverse contact ratios $Q_t < 2$, window functions $\sigma(\xi)$ with spans S larger than those indicated in Table 2 as a function of total contact ratio will be required. Eq. (27) can be solved to yield the normalized window span S/Δ as a function of F,

$$\frac{S}{\Delta} = \frac{4}{1-F}. \tag{30}$$

A simple example illustrates how a sensible span S can be chosen in these small contact ratio cases. Consider a gear with N=50 teeth. Suppose it is desired to have approximately N'=10 rotational harmonics, or slightly fewer, available for analysis between each pair of tooth-meshing harmonics. Then, the approximate fraction F of available rotational harmonics is $F \approx (10/50)=1/5$. Substituting this value into Eq. (30) yields $(S/\Delta)=5$. A window-function span of total duration $S=5\Delta$ of five base pitches would be required in this case, as indicated in Table 2. Hence, for this example, only a modest compromise in spatial resolution S has yielded a sensible number of rotational harmonics for use in the detection metric, Eq. (9), or its median counterpart.

If the above-described window function is shifted by steps of $S/4$, as suggested earlier, then the total number of step locations x_k required in this example would be $N\Delta/(5\Delta/4)=(4/5)N=40$ for the gear with 50 teeth. One or a few of these windowed examinations sequently rising above its neighbors would be an indication of localized damage.

However, in this spur-gear example, if $Q_t > 5/3$, then for the window-function S to fully capture damage on a single tooth, the value of S given by Eq. (28) would be used, as indicated by Table 2.

4.4. Gears with "negligible" manufacturing errors

All real gears have manufacturing errors, including the above-described class (3) errors. Moreover, a manufacturing error on the working surface of a single tooth will cause a non-zero contribution to every rotational harmonic of the STE vibration excitation caused by that gear, as shown in Appendix A or Eq. (A.4) of [3].

Suppose the error on this single tooth is a tooth-spacing error such that the tooth is caused to carry more loading than the other teeth on the gear. If this tooth begins to fail in bending fatigue, and either plastically deforms [16] or develops a root crack, the initial effect of this bending-fatigue damage will be to reduce the initial tooth-spacing error of the loaded tooth, which would result in a *reduction* in the transmission-error contribution from that tooth, and a *reduction* in the resultant rotational-harmonic contributions of the original spacing error. Hence, in order to detect damage at its earliest possible stage, the metrics of Eqs. (5)–(10) utilize only changes, either increases or decreases, in the individual rotational-harmonic amplitudes.

Table 2
Useful fractional values F, Eq. (29), of rotational-harmonic regions between adjacent tooth-meshing harmonics illustrated in Fig. 2 as a function of total contact ratio Q_t+Q_a, and associated values, Eq. (28), of normalized span S/Δ of window function $\sigma(\xi)$, Eq. (12).

Q_t+Q_a	4/3	3/2	5/3	2	3	4	6	8
F	0	1/9	1/5	1/3	5/9	2/3	7/9	5/6
S/Δ	4	9/2	5	6	9	12	18	24

A simple metric that would detect such changes is the average over rotational-harmonic number n of the *absolute value* of the differences in the synchronous-average transducer-response rotational-harmonic amplitudes, Eq. (7), i.e.,

$$AAD \triangleq \underset{over\ n}{average} |\delta|\alpha_y(n)||, \tag{31a}$$

$$AAD = \underset{over\ n}{average} ||\alpha_y(n)|_a - |\alpha_y(n)|_b|, \tag{31b}$$

where the averages should be taken only over the rotational-harmonic regions normally dominated by the class (3) manufacturing errors, as described earlier. If windowing is utilized, the windowed counterparts $|\alpha_z(n; x_k)|$ to the rotational-harmonic amplitudes $|\alpha_y(n)|$ should be used in Eqs. (31a) and (31b).

The above metric AAD does not depend on the existence of non-zero rotational-harmonic amplitudes $|\alpha_y(n)|_b$, as does ALR, Eq. (9). However, utilizing the ratios $|\alpha_y(n)|_a/|\alpha_y(n)|_b$ in ALR, Eq. (9), has the considerable advantage of normalizing the effect of the combined structural-path and transducer transfer functions, and partially normalizing the effects of the gear-meshing-action mesh transfer functions, as described earlier. These normalizations provide a considerable extension of the rotational-harmonic range over which useful averages can be taken.

5. Application to ring-gear seeded-fault detection

To ascertain the detectability of bending-fatigue damage on the ring gear of planetary gear systems using fixed accelerometers mounted on or near the ring gear, a seeded-fault test was carried out on the ring gear of the University of Maryland (planetary) Transmission Test Rig (PTTR). The steel ring gear has an outside diameter of 18.1 cm ($7\frac{1}{8}$ in), a root diameter of 14.9 cm ($5\frac{7}{8}$ in), and tooth height of 0.48 cm (3/16 in). The ring gear has 71 teeth and each of the three planet pinions has 22 teeth. Because 71 is a prime number, the ring-gear/planet pinions are hunting-tooth gear pairs. The contact ratio Q_t of the ring-gear/planet-pinion (internal) spur-gear meshes is about $4\frac{1}{4}$.

To simulate bending-fatigue cracks, notches were cut in the root location of a single ring-gear tooth on the tension side of the tooth. Two detectability test sets were run, one set with a notch depth of about 20 percent of the tooth-root thickness, and later, a second set with a notch depth of about 50 percent of the tooth-root thickness. This deeper notch was made on the same tooth as the 20 percent notch, by extending that notch to a 50 percent depth.

Three accelerometers were mounted on the ring gear. Accelerometer 1 was mounted directly adjacent to the notched tooth, and accelerometers 2 and 3 were mounted at 90° intervals from the notched tooth on the ring gear, one on either side of the tooth, which placed them 180° apart on the ring gear.

The gears involved in these tests were good-quality industrial gears. Standard tooth-spacing, profile, and lead measurements were made on the teeth with dedicated gear metrology equipment. The typical tooth-spacing (pitch) error between adjacent teeth on the ring gear was about 3 μm (120 microinches) with similar variation in measured tooth profiles. The largest adjacent tooth-spacing error was about 10 μm (400 microinches). Such tooth-to-tooth variations from equispaced perfect involute teeth are the above-described class (3) errors that cause the transmission-error rotational-harmonic amplitudes observed in transmission-error spectra between groups of so-called sidebands adjacent to the tooth-meshing harmonics. The error on *each* of the 71 ring-gear teeth provides a contribution to *all* of the STE rotational-harmonic amplitudes arising from the above-described class (3) manufacturing errors. The error contribution from the loaded notched tooth should be somewhat larger than that from most of the other 70 teeth, but the collective rotational-harmonic contributions from the manufacturing errors on the other 70 teeth would be expected to be significantly larger than the rotational-harmonic contributions from the single notched tooth. Hence, the metric ALR, Eq. (9), has been used to detect *changes* in the *individual* rotational-harmonic amplitudes.

Because the present detection example was applied to seeded-fault damage on a fixed ring gear monitored by fixed accelerometers mounted on the ring gear, no simple convenient method was available for the above-described windowing. (At every instant, each fixed accelerometer was experiencing an excitation arising from *all three* planet/ring-gear meshes, thereby not permitting localized windowing of the excitation arising from only a *single* ring-gear location.) Therefore, manufacturing-error contributions arising from all 71 teeth on the gear were providing STE rotational-harmonic contributions. However, especially for the accelerometer mounted adjacent to the notched tooth, attenuation of the structural transfer function between distant teeth and that accelerometer provided some of the effects [36] that windowing would have provided.

Because the contact ratio Q_t of the ring-gear/planet-pinion meshes was about 4 1/4, deflections of the notched tooth under significant applied torques always were supported by the other three teeth also simultaneously in contact. Therefore, even under very heavy torques, deflections of the notched tooth were limited to the amount of the deflections of the other three teeth in contact at the same time.

5.1. Synchronous averaging and choice of rotational harmonics

As described above and in [16], the STE vibration-excitation rotational-harmonic contributions from one gear of a hunting-tooth gear pair can be eliminated by utilizing, in synchronous averages, the number of contiguous rotation segments of the gear of interest equal to an integer multiple of the number of teeth on the mating gear. The ring gear is the gear of interest in the present case, and the fundamental period of its rotational-harmonic contributions is the planet-carrier rotation period (by placing the "observer" on a planet pinion axis). Hence, to eliminate the planet-pinion rotational-harmonic contributions in synchronous averages of accelerometer responses, an integer multiple (4) of 22 contiguous planet-carrier rotation segments was utilized in the accelerometer-response synchronous average—i.e., 88 such contiguous planet-carrier rotation segments.

Fourier analysis of the synchronous averages of accelerometer responses was carried out yielding the rotational-harmonic amplitudes of the synchronous averages. If each of the three planets carries the same loading, then ring-gear manufacturing errors and tooth damage will contribute only to those planet-carrier (ring-gear) rotational harmonics that are integer multiples of three times the planet-carrier rotational fundamental harmonic [36,37]. (Errors on the ring gear cause ring-gear rotational-harmonic contributions.) Hence, in all applications reported on herein, only these integer multiples of three planet-carrier rotational-harmonic amplitudes were utilized in computations of the ALR detection metric, Eq. (9).

Because the ring gear has 71 teeth, there are 70 rotational harmonics between each pair of tooth-meshing harmonics. But $\frac{70}{3} = 23\frac{1}{3}$. Hence, between each pair of tooth-meshing harmonics there are either 23 or 24 rotational harmonics that are integer multiples of 3. In order to avoid the "sideband harmonics" caused by the above-described class (2) errors, it was initially decided to utilize 18 of these 23 or 24 available integer multiples of 3, where the locations of these 18 rotational harmonics were approximately centered between the tooth-meshing harmonic locations on either side of the 18. However, unusually strong sideband harmonics were observed in the rotational-harmonic amplitudes just below the 2nd tooth-meshing harmonic, which is rotational-harmonic number 142. Consequently, an additional 4 of these integer multiple of 3 rotational harmonics were eliminated in this harmonic-number region. All other integer multiples of 3 rotational harmonics between rotational-harmonic zero and the 4th tooth-meshing harmonic, which is rotational-harmonic $4 \times 71 = 284$, were used in the damage-detection metric ALR, Eq. (9), as indicated above. Thus, the rotational-harmonic spans used were integer multiples of 3 within the rotational-harmonic-number spans 9–60, 81–120, 153–204, and 222–273 yielding a total of 18+14+18+18=68 rotational-harmonic amplitudes used to carry out the average indicated in the ALR detection metric, Eq. (9).

In *each* of the above-described four harmonic-number spans, the detection metric ALR, Eq. (9), was computed by evaluating $|\alpha_y(n)|_b$ computed from synchronous averages of the before-notch (healthy) ring-gear accelerometer measurements and then by evaluating $|\alpha_y(n)|_a$ from synchronous averages of the after 20 percent notch ring-gear accelerometer measurements. The ALR metric also was evaluated comparing the before-notch case and the after 50 percent notch case. These comparisons were carried out for seven torque values from 40 percent to 100 percent of full torque, in increments of 10 percent. In each of the four above-described harmonic-number spans, the computed ALR detection metric was consistently larger for the 50 percent notch computations than for the 20 percent notch computations. Similar computations for rotational-harmonic spans beyond the 4th tooth-meshing harmonic showed less consistency, where the 50 percent notch ALR value was occasionally smaller than the 20 percent notch ALR value. Hence, our final computations of the ALR values utilized only the above-described 68 rotational-harmonic amplitudes obtained from rotational-harmonic computations below the 4th tooth-meshing harmonic. The results of these computations are presented and discussed below.

5.2. Loading variability of ALR metric referenced to fixed loading

Because the STE vibratory excitation is a displacement form of excitation and manufacturing errors are geometric (displacement) errors, the dominant cause of changes in the class (3) error rotational-harmonic amplitudes, with changes in gear loading, is changes in contact regions on the individual teeth due to the loading changes. These contact-region changes occur as a result of tip relief, root relief, axial crowning, etc. To understand the effects on the rotational-harmonic amplitudes of changes in gear loading, the ALR metric was computed as a function of gear loading from accelerometer data obtained from the ring gear with unnotched tooth, with 20 percent tooth notch, and with 50 percent tooth notch. Synchronous averages of accelerometer outputs were carried out in each case as explained above. In each case, the reference ("before") rotational-harmonic amplitudes $|\alpha_y(n)|_b$ were the amplitudes obtained at 40 percent of full torque, and the "after" amplitudes $|\alpha_y(n)|_a$ were amplitudes obtained at successively higher torque values of 50 percent, 60 percent, …, 100 percent, in increments of 10 percent. Hence, the only change between each "before" and each "after" measurement was a change in torque from the 40 percent torque value. All measurements were made at 300 RPM.

These results are shown in Figs. 3a–c. Because the change in any rotational-harmonic amplitude, increase or decrease, always is treated as positive in the ALR metric, Eq. (9); see Eq. (5); each curve is generally increasing with increased torque (except between 90 percent and 100 percent torque in the 50 percent notch case for Accel 1 in Fig. 3c). Because the contact regions on the individual teeth increase with increases in loading, this behavior is as one would expect.

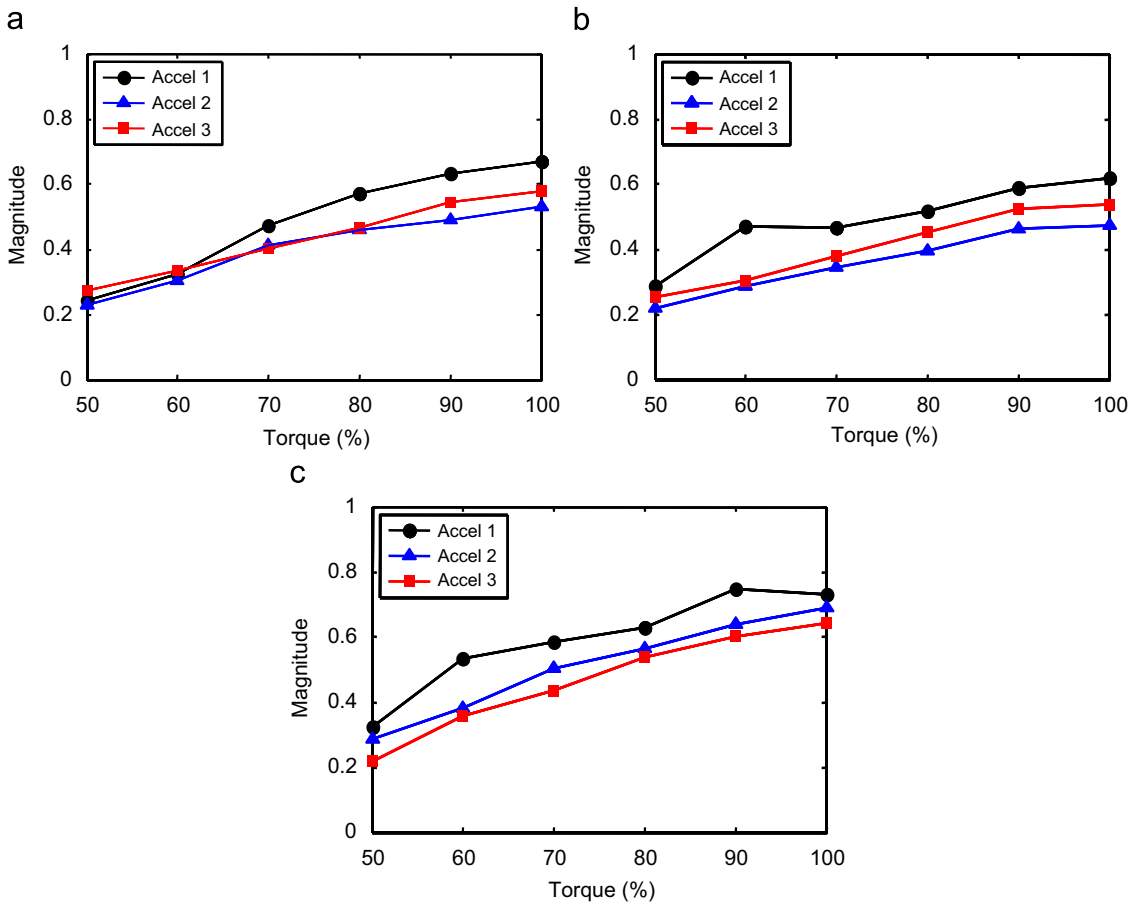

Fig. 3. ALR detection metric, Eq. (9), computed as a function of gear loading. In each of (a)–(c), the reference "before" rotational-harmonic amplitudes $|\alpha_y(n)|_b$ were the amplitudes obtained at 40 percent of full torque and the "after" amplitudes $|\alpha_y(n)|_a$ were amplitudes obtained at successively higher torque values of 50 percent, 60 percent, …, 100 percent in increments of 10 percent: (a) computed for unnotched tooth; (b) computed for 20 percent notch depth; (c) computed for 50 percent notch depth. Rotational-harmonic spans utilized were between 0th and 4th tooth-meshing harmonic as described in main text.

However, the overall slopes of the results for the unnotched, 20 percent notch, and 50 percent notch cases all are about the same. Consider the 50 percent notch case. When the notched tooth is in contact with the teeth of a mating pinion, it should elastically deform more than the same tooth with no notch. The effect of this increased elastic deformation is to increase the rotational-harmonic changes caused by the increased elastic deformation of all teeth in contact. But simultaneously, the reduced composite stiffness of all teeth in contact will result in a small increase in the operating contact ratio—i.e., the contact regions of all teeth in contact relative to the contact regions that would occur with no notch. Increases in contact ratio cause reductions in rotational-harmonic amplitudes. Thus, the effects on the rotational-harmonic amplitudes of the increase in elastic deformation of the notched tooth and the increase in contact ratio caused by this increase in elastic deformation tend to compensate for one another. This may explain why the overall slopes of the curves in all three Figs. 3a–c have the same general behavior. Moreover, the increased-contact-ratio effect also may explain the slight decrease in ALR in going from 90 percent to 100 percent torque in the 50 percent notch case for Accel 1 in Fig. 3c.

5.3. *Before notch and after notch ALR metric detection results*

Figs. 4a–c show the before notch and after notch ALR results obtained for the three accelerometer locations. Each figure shows the ALR metric, Eq. (9), computed using unnotched-tooth values $|\alpha_y(n)|_b$ and 20 percent notch values $|\alpha_y(n)|_a$ as one curve, and the unnotched-tooth values $|\alpha_y(n)|_b$ and 50 percent notch values $|\alpha_y(n)|_a$ as a second curve. The same torque value was used for the unnotched and notched computation at each of the indicated torques.

For each of the three accelerometer locations, the 50 percent notch ALR value is, for all torques, larger than the 20 percent notch ALR value, as one would expect. Moreover, the accelerometer 2 and accelerometer 3 values of the ALR computations are consistently below the accelerometer 1 values. This also is as one would expect, because the

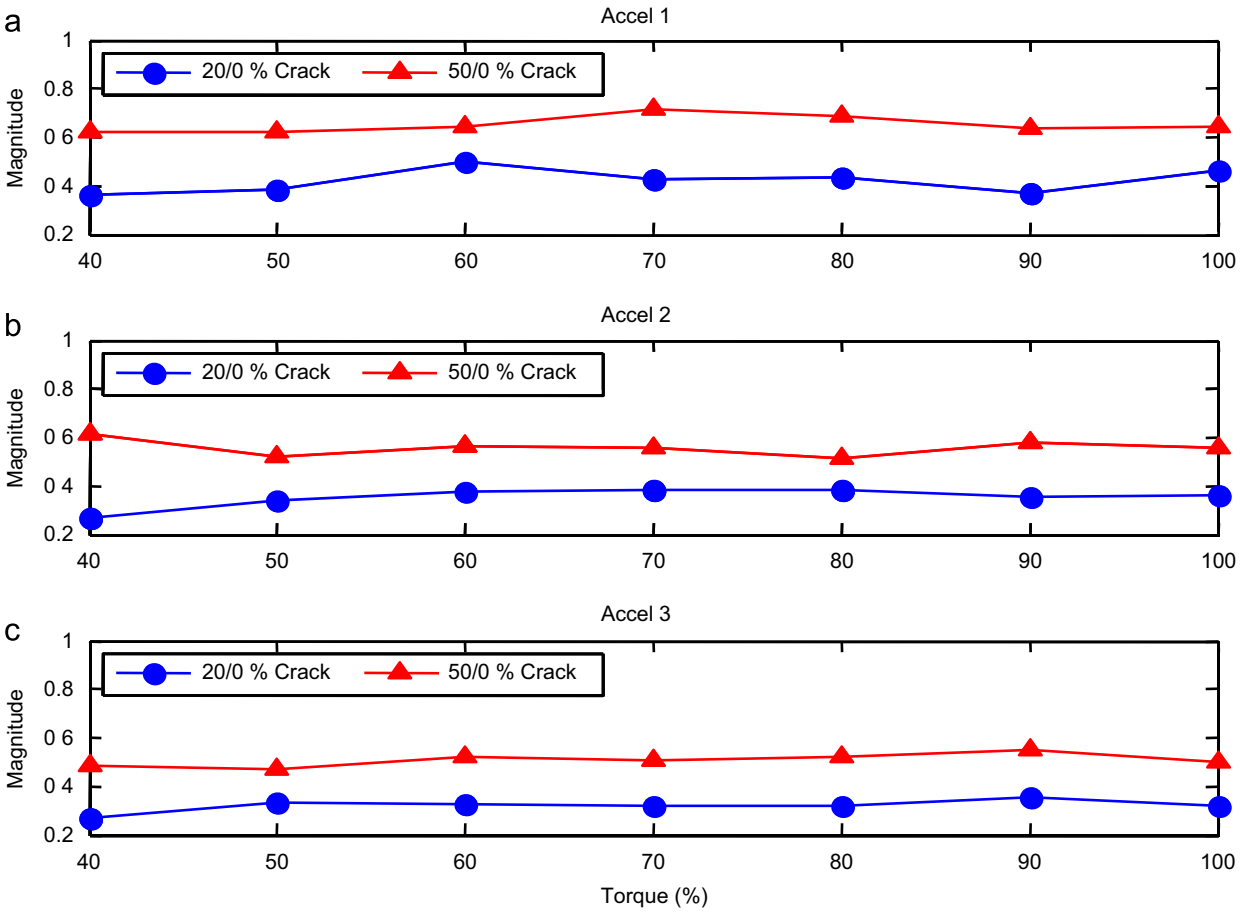

Fig. 4. ALR detection metric, Eq. (9), computed from before-notch and after-notch rotational-harmonic amplitudes $|\alpha_y(n)|_b$ and $|\alpha_y(n)|_a$, respectively, as a function of gear loading. Each plot displays before-notch versus 20 percent notch depth and before-notch versus 50 percent notch depth. (a), (b), (c), computed, respectively, from accelerometer (1), (2), (3) rotational harmonics.

accelerometer 2 and 3 locations were placed farther from the notched tooth than the accelerometer 1 location, which was directly adjacent to the notched tooth.

In each of Figs. 4a–c, the ALR values show no consistent trend with increasing torque. This behavior is consistent with the results shown in Figs. 3a–c and is likely explained by the expected increase in operating contact ratio caused by the reduced composite mesh stiffness caused by the notched tooth. This increase in operating contact ratio presumably compensates for the otherwise-expected increase in rotational-harmonic amplitude changes caused by the notched tooth, as explained above in the context of Figs. 3a–c.

After making the accelerometer measurements for the unnotched tooth case, the ring gear was removed from its mounting place, and the 20 percent notch was cut on the tooth as explained earlier. Then the ring gear was re-mounted and the accelerometer measurements were made for the 20 percent notch case. The ring-gear was again removed, the notch extended to 50 percent depth, then the ring gear was re-mounted for the third set of accelerometer measurements. Because of this removal and re-mounting of the ring gear, we cannot be *certain* that all of the differences shown in Figs. 4a–c are attributable to the increase in rotational-harmonic-amplitude changes caused by the notch and resultant changes in operating contact ratio. Some of the observed changes *might* have been caused by changes arising from the removal and re-mounting of the ring gear. However, all of the results appear to be consistent with this latter possibility not being the dominant cause of the observed changes. In particular, for each of the results shown in Figs. 3a–c, no removal of the ring gear was involved between the before $|\alpha_y(n)|_b$ and after $|\alpha_y(n)|_a$ rotational-harmonic computations in each of the three figures. Yet the overall slopes in all three of these figures exhibit the same general behavior. Even if some of the changes in Figs. 4a–c, with differing notch depths, were caused by removal and re-mounting of the ring gear, it nevertheless has been shown that the ALR detection metric is extremely sensitive to changes in rotational-harmonic amplitudes, which are very sensitive to tooth-damage, which is what we wished to show.

In the above-described ring-gear application, inconsistent behavior was observed in the rotational-harmonic-number region beyond the 4th tooth-meshing harmonic, as described in Section 5.1. Because waveform-processing errors, or variations in structural/transducer transfer functions, are likely to degrade the high-frequency (large rotational-harmonic

number) regions more than the lower-frequency regions, one can expect an upper bound in rotational-harmonic number beyond which the above-described detection metrics may not be reliable. In particular, it is possible that removal of the ring gear for notch creation and notch depth increase, in the above-described application, was a cause of sufficient changes in structural transfer functions between meshing locations and accelerometer locations to account for the inconsistent behavior observed beyond the 4th tooth-meshing harmonic.

In the operational application of the ALR metric, Eq. (9), to detect gear damage, no gear removal normally would be required between making "before" and "after" computations of accelerometer-response rotational-harmonic amplitudes. Hence, the above-described uncertainty, pertaining to possible changes caused by gear removal, would not be relevant in operational applications of this detection method.

As mentioned earlier, in addition to the effects of structural/transducer transfer functions $H(n)$, Eq. (2), the meshing action of helical and high-contact-ratio spur gears has a substantial attenuating effect on tooth deviations, especially in the high-harmonic-number region. By dealing with the amplitude ratios, Eq. (4), some of these mesh-attenuating effects are compensated for. However, the meshing-action attenuation of any individual rotational harmonic will be changed by gear-tooth damage. Because such changes will cause changes in the values of the rotational-harmonic amplitude ratios, Eq. (4), such changes in meshing-action attenuation should not significantly degrade the potential for damage detections.

6. Summary

A simple algorithm, ALR, Eq. (9), or its median counterpart, MLR, has been suggested for very early frequency-domain detection of damage on teeth of meshing gears. This algorithm utilizes rotational-harmonic amplitudes $|\alpha_y(n)|$ of transducer responses caused by class (3) gear manufacturing errors and potential tooth damage. Ratios $|\alpha_y(n)|_a/|\alpha_y(n)|_b$ of after potential damage and before potential damage rotational-harmonic amplitudes are used, which eliminates effects of rotational-harmonic amplitude changes caused by transducer and structural path between tooth-meshing location and transducer output, and minimizes effects of amplitude changes caused by gear-meshing multiple-tooth contact, thereby normalizing resultant rotational-harmonic amplitudes to allow statistical averaging over a large range of available rotational harmonics. Due to the contributions of manufacturing errors, early tooth damage will cause either increases or decreases in individual rotational-harmonic amplitudes with almost equal probability. Hence, absolute values of logarithm of the ratio $|\alpha_y(n)|_a/|\alpha_y(n)|_b$, Eq. (5), are used to equally weight either increases or decreases in rotational-harmonic amplitudes. Use of the natural logarithm permits simple interpretation of computed ALR results, Eqs. (6)–(9), or the median counterpart MLR, while minimizing effects of outliers, Table 1. Synchronous averaging tailored to the meshing gear pair is utilized to minimize effects of noise and rotational-harmonic contributions of the mating gear [16]. For gears with "negligible" manufacturing errors, an alternative detection metric, AAD, Eq. (31), was suggested.

Time-windowing, Eqs. (11) and (12) with $S \approx 3(Q_t+Q_a)\Delta$, Eq. (28), tailored to the total contact ratio Q_t+Q_a of the meshing gear pair, was developed to isolate individual tooth locations, thereby allowing damage detections based on threshold exceedances. Unavoidable reductions in available rotational harmonics useful for detection purposes caused by windowing, Eq. (29), Fig. 2, and Table 2, were delineated.

The ALR metric, Eq. (9), was utilized to successfully detect seeded tooth-bending-fatigue faults provided by a 20 percent of tooth thickness root notch and a 50 percent of tooth thickness root notch, Fig. 4. This test was carried out on a ring-gear tooth of a small planetary gear system utilizing no windowing.

Acknowledgements

This work was partially supported by the Defense Advanced Research Projects Agency (DARPA) under subcontract to Northrop-Grumman Systems Corporation; program title "Structural Integrity Prognosis System." Approved for Public Release, Distribution Unlimited. The present topic was suggested to the authors by Steve Engel of Northrop-Grumman. The support for this work is gratefully acknowledged.

Appendix A. Contributions to STE rotational-harmonic spectra caused by deviations of individual tooth working surfaces from the mean working surface

Denote the deviation of the working surface of a generic tooth j from the mean working surface by $\varepsilon_j(y, z)$, where y and z are rectangular coordinates describing location on the working surface [2, Eq. (50)]. The deviations $\varepsilon_j(y, z)$ are the class (2) and (3) working surface errors (and damage) described in Section 3.1. Such surface deviations on a gear with N teeth can be represented as a superposition of (orthogonal) functions $\psi_m(y, z)$, m=0, 1, 2,…, e.g., [2, Eq. (131),7, Eqs. (81), (82)]

$$\varepsilon_j(y,z) = \sum_m b_{j,m}\psi_m(y,z). \tag{A.1}$$

Define [2, Eq. (135)]

$$B_m(n) \triangleq \frac{1}{N}\sum_{j=0}^{N-1} b_{j,m}\exp(-i2\pi nj/N), \tag{A.2}$$

which is the (discrete) Finite Fourier Transform [38] of the sequence of expansion coefficients $b_{j,m}$. The STE rotational-harmonic Fourier series coefficients of the tooth-deviation contributions $\varepsilon_j(y, z)$, $j=0, 1, \ldots, N-1$ can be expressed [2, Eq. (134)] as

$$\alpha_\zeta(n) = \sum_m B_m(n)\hat{\phi}_m[n/(N\Delta)], \tag{A.3}$$

where the functions $\hat{\phi}_m[n/(N\Delta)]$ are the "mesh transfer functions" [2, Eq. (123)] associated with the choice of expansion functions $\psi_m(y, z)$. The functions $B_m(n)$, Eq. (A.2), satisfy the periodic property [2, Eqs. (143), (144))],

$$B_m(n+pN) = B_m(n), \quad p = 0, \pm 1, \pm 2, \ldots \tag{A.4}$$

due to the discrete nature of gear teeth.

Suppose now that the working surface of a particular tooth $j=j'$ experiences damage. The change in this (loaded) working surface caused by damage also can be represented using the same set of expansion functions $\psi_m(y, z)$. Denote the expansion coefficients of the change in the damaged working surface of tooth j' by $b'_{j'm}$. Then, by using the Kronecker delta symbol $\delta_{j,j'}$ [39, p. 480], after this damage occurs, $B_m(n)$, Eq. (A.2), can be expressed as

$$\begin{aligned} B'_m(n) &= \frac{1}{N}\sum_{j=0}^{N-1}[b_{j,m} + b'_{j',m}\delta_{j,j'}]\exp(-i2\pi nj/N) \\ &= B_m(n) + \frac{1}{N}b'_{j',m}\exp(-i2\pi nj'/N), \end{aligned} \tag{A.5}$$

according to Eq. (A.2). Substituting $B'_m(n)$ into Eq. (A.3) yields an expression for the STE rotational-harmonic Fourier series coefficients $\alpha'_\zeta(n)$ after damage on tooth j' has occurred,

$$\alpha'_\zeta(n) = \alpha_\zeta(n) + \left\{\frac{1}{N}\sum_m b'_{j',m}\hat{\phi}_m[n/(N\Delta)]\right\}\exp(-i2\pi nj'/N), \tag{A.6a}$$

$$\alpha'_\zeta(n) = \alpha_\zeta(n) + \delta\alpha_\zeta(n), \tag{A.6b}$$

where the change in the STE Fourier series coefficients $\alpha_\zeta(n)$ caused by damage on tooth j' is

$$\delta\alpha_\zeta(n) \triangleq \left\{\frac{1}{N}\sum_m b'_{j',m}\hat{\phi}_m[n/(N\Delta)]\right\}\exp(-i2\pi nj'/N). \tag{A.7}$$

There are two sources of rotational-harmonic variability of the tooth-damage change $\delta\alpha_\zeta(n)$ in the STE Fourier series coefficients $\alpha_\zeta(n)$: variability caused by the complex exponential in Eq. (A.7), and variability caused by the mesh transfer functions $\hat{\phi}_m[n/(N\Delta)]$. The variability with n caused by the complex exponential arises directly from the tooth-number location j' of the damage in the working surface of tooth j' [2]. The variability caused by the mesh transfer functions $\hat{\phi}_m[n/(N\Delta)]$ is caused by the attenuating effects of multiple-tooth contact. The functions $\hat{\phi}_m[n/(N\Delta)]$ are real and typically reverse sign often with increasing rotational-harmonic number, e.g. [7;9, Eq. (21.47)]. The locations of these reversals are strongly dependent on the gear-mesh transverse contact ratio Q_t, and in the case of helical gears, the axial contact ratio Q_a also. As a consequence of the above two sources of rotational-harmonic variability, damage on a generic gear tooth j' will cause fluctuating increases and decreases in STE rotational-harmonic amplitudes with increasing rotational-harmonic number n. These virtually unpredictable fluctuations will occur out to arbitrarily large harmonic numbers, n; see Eq. (A.4). As a consequence of these damage-caused fluctuations in STE rotational-harmonic amplitudes, the suggested detection metric of Eqs. (5)–(9) utilizes changes, either increases or decreases, in the individual amplitudes of the rotational-harmonic spectra $\alpha_y(n)$.

Appendix B. Fourier series coefficients of $\sigma(\xi)$, Eq. (12)

The Fourier series coefficients, Eq. (13a), of the window function $\sigma(\xi)$, Eq. (12), are with

$$a = 2\pi/S, \tag{B.1}$$

$$\gamma_\sigma(n) = \frac{1}{N\Delta}\int_{-N\Delta/2}^{N\Delta/2}\sigma(\xi)\exp[-i2\pi n\xi/(N\Delta)]\,d\xi, \tag{B.2a}$$

$$\gamma_\sigma(n) = \frac{1}{2N\Delta}\int_{-\pi/a}^{\pi/a}[1+\cos(a\xi)]\cos[2\pi n\xi/(N\Delta)]\,d\xi, \tag{B.2b}$$

since $\sigma(\xi)$ is real and an even function of ξ. Define

$$I_1 \triangleq \frac{1}{N\Delta}\int_{-\pi/a}^{\pi/a} \cos[2\pi n\xi/(N\Delta)]\, d\xi, \tag{B.3}$$

$$I_2 \triangleq \frac{1}{N\Delta}\int_{-\pi/a}^{\pi/a} \cos(a\xi)\cos[2\pi n\xi/(N\Delta)]\, d\xi. \tag{B.4}$$

Then, with $a=2\pi/S$, Eq. (B.1), there follows from Eqs. (B.2b)–(B.4),

$$\gamma_\sigma(n) = \tfrac{1}{2}(I_1+I_2). \tag{B.5}$$

I_1 is an elementary integral,

$$I_1 = \frac{1}{N\Delta}\frac{1}{2\pi n/(N\Delta)}\sin[2\pi n\xi/(N\Delta)]_{-\pi/a}^{\pi/a} = \frac{1}{\pi n}\sin[2\pi^2 n/(aN\Delta)], \tag{B.6}$$

since the sine function is an odd function. I_2 is also an elementary integral [39, p. 805],

$$\begin{aligned} I_2 &= \frac{1}{N\Delta}\left[\frac{\sin\left(a-(2\pi n/N\Delta)\right)\xi}{2\left(a-(2\pi n/N\Delta)\right)} + \frac{\sin\left(a+(2\pi n/N\Delta)\right)\xi}{2\left(a+(2\pi n/N\Delta)\right)}\right]_{-\pi/a}^{\pi/a}, \quad a^2 \neq \left(\frac{2\pi n}{N\Delta}\right)^2 \\ &= \frac{1}{N\Delta}\left[\frac{\sin\left(\pi-(2\pi^2 n/aN\Delta)\right)}{\left(a-(2\pi n/N\Delta)\right)} + \frac{\sin\left(\pi+(2\pi^2 n/aN\Delta)\right)}{\left(a+(2\pi n/N\Delta)\right)}\right], \end{aligned} \tag{B.7}$$

where we again have used the fact that the sine function is an odd function. But

$$\sin\left(\pi \pm \frac{2\pi^2 n}{aN\Delta}\right) = \sin\pi\cos\frac{2\pi^2 n}{aN\Delta} \pm \cos\pi\sin\frac{2\pi^2 n}{aN\Delta} = 0 \mp \sin\frac{2\pi^2 n}{aN\Delta}. \tag{B.8}$$

Substituting Eq. (B.8) into Eq. (B.7), one has

$$\begin{aligned} I_2 &= \frac{1}{N\Delta}\left[\frac{\sin(2\pi^2 n/aN\Delta)}{\left(a-(2\pi n/N\Delta)\right)} - \frac{\sin(2\pi^2 n/aN\Delta)}{\left(a+(2\pi n/N\Delta)\right)}\right] \\ &= \frac{\sin(2\pi^2 n/aN\Delta)}{N\Delta}\left[\frac{1}{a-(2\pi n/N\Delta)} - \frac{1}{a+(2\pi n/N\Delta)}\right]. \end{aligned} \tag{B.9}$$

However,

$$\frac{1}{x-y} - \frac{1}{x+y} = \frac{x+y-(x-y)}{(x-y)(x+y)} = \frac{2y}{x^2-y^2}. \tag{B.10}$$

Applying Eq. (B.10) to Eq. (B.9), there follows:

$$\begin{aligned} I_2 &= \frac{\sin(2\pi^2 n/aN\Delta)}{N\Delta}\left[\frac{4\pi n/(N\Delta)}{a^2-(4\pi^2 n^2/(N\Delta)^2)}\right] \\ &= \frac{\sin(2\pi^2 n/aN\Delta)}{(N\Delta)^2}\left[\frac{4\pi n}{a^2-4\pi^2 n^2/(N\Delta)^2}\right] \\ &= \sin\frac{2\pi^2 n}{aN\Delta}\left[\frac{4\pi n}{(aN\Delta)^2-4\pi^2 n^2}\right]. \end{aligned} \tag{B.11}$$

Using Eqs. (B.6) and (B.11),

$$I_1+I_2 = \sin\frac{2\pi^2 n}{aN\Delta}\left[\frac{1}{\pi n} + \frac{4\pi n}{(aN\Delta)^2-(2\pi n)^2}\right]. \tag{B.12}$$

But,

$$\begin{aligned} \frac{1}{\pi n} + \frac{4\pi n}{(aN\Delta)^2-(2\pi n)^2} &= \frac{(aN\Delta)^2-(2\pi n)^2+4\pi^2 n^2}{\pi n[(aN\Delta)^2-(2\pi n)^2]} \\ &= \frac{(aN\Delta)^2}{\pi n[(aN\Delta)^2-(2\pi n)^2]} \\ &= \frac{1}{\pi n[1-(2\pi n/aN\Delta)^2].} \end{aligned} \tag{B.13}$$

Therefore, combining Eqs. (B.5), (B.12), (B.13), and then Eq. (B.1),

$$\gamma_\sigma(n) = \frac{\sin[2\pi^2 n/(aN\Delta)]}{2\pi n\{1-[2\pi n/(aN\Delta)]^2\}} = \frac{\sin[\pi(S/\Delta)(n/N)]}{2\pi n\{1-[(S/\Delta)(n/N)]^2\}}, \quad n = 0, \pm 1, \pm 2, \ldots, \tag{B.14}$$

which is the result, Eq. (13b).

References

[1] R.J. Drago, Fundamentals of Gear Design, Butterworths, Boston, 1988.
[2] W.D. Mark, Analysis of the vibratory excitation of gear systems: basic theory, Journal of Acoustical Society of America 63 (1978) 1409–1430.
[3] W.D. Mark, C.P. Reagor, Static-transmission-error vibratory-excitation contributions from plastically deformed gear teeth caused by tooth bending-fatigue damage, Mechanical Systems and Signal Processing 21 (2007) 885–905.
[4] S.L. Harris, Dynamic loads on the teeth of spur gears, Proceedings of the Institution of Mechanical Engineers 172 (1958) 87–100.
[5] R.W. Gregory, S.L. Harris, R.G. Munro, Dynamic behavior of spur gears, Proceedings of the Institution of Mechanical Engineers 178 (1963–1964) 207–218.
[6] H.K. Kohler, A. Pratt, A.M. Thompson, Dynamics and noise of parallel-axis gearing, Proceedings of the Institution of Mechanical Engineers 184 (1969–1970) 111–121.
[7] W.D. Mark, Analysis of the vibratory excitation of gear systems, II: tooth error representations, approximations, and application, Journal of the Acoustical Society of America 66 (1979) 1758–1787.
[8] W.D. Mark, The role of the discrete Fourier transform in the contribution to gear transmission error spectra from tooth-spacing errors, Proceedings of the Institution of Mechanical Engineers 201 (Part C) (1987) 227–232.
[9] W.D. Mark, Elements of gear noise prediction, in: L.L. Beranek, I.L. Ver (Eds.), Noise and Vibration Control Engineering: Principles and Applications, 1992, pp. 735–770 (Chapter 21).
[10] R.M. Stewart, Some useful data analysis techniques for gearbox diagnostics, Report MHM/R/10/77, University of Southampton, Institute of Sound and Vibration Research, 1977.
[11] P.D. McFadden, Examination of a technique for the early detection of failure in gears by signal processing of the time domain average of the meshing vibration, Mechanical Systems and Signal Processing 1 (1987) 173–183.
[12] R.A. Thompson, B. Weichbrodt, Gear diagnostics and wear detection, ASME, 1969 (Paper 69-VIBR-10).
[13] B. Weichbrodt, K.A. Smith, Signature analysis—nonintrusive techniques for incipient failure identification, General Electric Technical Information Series (1970) (Paper 70-C-364).
[14] S. Braun, The extraction of periodic waveforms by time domain averaging, Acoustica 32 (1975) 69–76.
[15] S.G. Braun, B.B. Seth, On the extraction and filtering of signals acquired from rotation machines, Journal of Sound and Vibration 65 (1979) 37–50.
[16] W.D. Mark, C.P. Reagor, D.R. McPherson, Assessing the role of plastic deformation in gear-health monitoring by precision measurement of failed gears, Mechanical Systems and Signal Processing 21 (2007) 177–192.
[17] W.J. Staszewski, G.R. Tomlinson, Local tooth fault detection in gearboxes using a moving window procedure, Mechanical Systems and Signal Processing 11 (1997) 331–350.
[18] W.D. Mark, Spectral analysis of the convolution and filtering of non-stationary stochastic processes, Journal of Sound and Vibration 11 (1970) 19–63.
[19] W.J. Wang, P.D. McFadden, Application of wavelets to gear vibration signals for fault detection, Journal of Sound and Vibration 192 (1996) 927–939.
[20] P. Loughlin, F. Cakrak, L. Cohen, Conditional moments analysis of transients with application to helicopter fault data, Mechanical Systems and Signal Processing 14 (2000) 511–522.
[21] Naim Baydar, Andrew Ball, A comparative study of acoustic and vibration signals in detection of gear failures using Wigner–Ville distribution, Mechanical Systems and Signal Processing 15 (2001) 1091–1107.
[22] C.J. Stander, P.S. Heyns, Using vibration monitoring for local fault detection on gears operating under fluctuating load conditions, Mechanical Systems and Signal Processing 16 (2002) 1005–1024.
[23] Xianfeng Fan, Ming J. Zuo, Gearbox fault detection using Hilbert and wavelet packet transform, Mechanical Systems and Signal Processing 20 (2006) 966–982.
[24] A. Belsak, J. Flasker, Method for detecting fatigue cracks in gears, Theoretical and Applied Fracture Mechanics 46 (2006) 105–113.
[25] M.A. Jafarizadeh, R. Hassannejad, M.M. Ettefagh, S. Chitsaz, A synchronous input gear damage diagnosis using time averaging and wavelet filtering, Mechanical Systems and Signal Processing 22 (2008) 172–201.
[26] R.B. Randall, A new method of modeling gear faults, ASME Journal of Mechanical Design 104 (1982) 259–267.
[27] P.D. McFadden, J.D. Smith, A signal processing technique for detecting local defects in a gear from the signal average vibration, Proceedings of the Institution of Mechanical Engineers 199 (Part C) (1985) 287–292.
[28] P.D. McFadden, Detecting fatigue cracks in gears by amplitude and phase demodulation of the meshing vibration, ASME Journal of Vibration, Acoustics, Stress, and Reliability in Design 108 (1986) 165–170.
[29] Shengxiang Jia, Ian Howard, Comparison of localized spalling and crack damage from dynamic modeling of spur gear vibrations, Mechanical Systems and Signal Processing 20 (2006) 332–349.
[30] J.H. Kuang, A.D. Lin, Theoretical aspects of torque responses in spur gearing due to mesh stiffness variation, Mechanical Systems and Signal Processing 17 (2003) 255–271.
[31] C. James Li, Hyungdae Lee, Gear fatigue crack prognosis using embedded model, gear dynamic model and fracture mechanics, Mechanical Systems and Signal Processing 19 (2005) 836–846.
[32] W.A. Gardner, Statistical Spectral Analysis: A Nonprobalistic Theory, Prentice-Hall, Englewood Cliffs, NJ, 1988.
[33] C. Capdessus, M. Sidahmed, Cyclostationary processes: application in gear faults early diagnosis, Mechanical Systems and Signal Processing 14 (2000) 371–385.
[34] Amani Raad, Jerome Antoni, Menad Sidahmed, Indicators of cyclostationarity: theory and application to gear fault monitoring, Mechanical Systems and Signal Processing 22 (2008) 547–587.
[35] A suggestion made by Michael Koelemay of Impact Technologies LLC.
[36] W.D. Mark, J.A. Hines, Stationary transducer response to planetary-gear vibration excitation with non-uniform planet loading, Mechanical Systems and Signal Processing 23 (2009) 1366–1381.
[37] P.D. McFadden, J.D. Smith, An explanation for the asymmetry of the modulation sidebands about the tooth meshing frequency in epicyclic gear vibration, Proceedings of the Institution of Mechanical Engineers 199 (Part C) (1985) 65–70.
[38] J.W. Cooley, P.A.W. Lewis, P.D. Welch, The finite Fourier transform, IEEE Transactions Audio Electroacoustics AU 17 (1969) 77–85 (Reprinted in Digital Signal Processing, L.R. Rabiner, C.M. Rader (Eds.), IEEE Press, New York, 1972, pp. 251–259).
[39] G.A. Korn, T.M. Korn, Mathematical Handbook for Scientists and Engineers, McGraw-Hill, New York, 1961.